863. Development of a finite element model of the sailplane fuselage

M. Andrikaitis[1], A. Fedaravičius[2]
Kaunas University of Technology, Kęstučio 27, 44312 Kaunas, Lithuania
E-mail: [1]*marius.andrikaitis@gmail.com*, [2]*algimantas.fedaravicius@ktu.lt*

(Received 5 July 2012; accepted 4 September 2012)

Abstract. This paper presents development of finite element model of sailplane LAK-17B fuselage, which will be used to demonstrate the compliance with requirements of strength, deformation, crashworthiness and flutter behavior. FE analysis may be used only if the structure conforms to those for which experience has shown the method to be reliable. LAK-17B is a modification of a certified sailplane LAK-17A. Compliance with strength requirements of this sailplane was confirmed by load tests. Data of these tests will be used to evaluate numerical model reliability. The article presents modeling principles used to create finite element models of the sailplanes LAK-17A and LAK-17B together with consideration of load evaluation procedure.

Keywords: finite element model, sailplane, fuselage.

Introduction

During sailplane certification process, compliance with strength and deformation requirements must be confirmed for each critical aircraft load condition. According to reference [1], finite element (FE) analysis may be used only if the structure conforms to those for which experience has shown this method to be reliable. In other cases, substantiating load tests must be conducted.

FE models of complete aircraft structures are primarily used to determine natural frequencies and modal shapes as well as to investigate flutter behavior and evaluate crashworthiness of the aircraft [2-4, 7-10]. Development of models representing the complete aircraft structures consist of complex CAD modeling and finite element meshing procedures.

This paper presents FE model development procedure for the sailplane LAK-17B fuselage that will be used to demonstrate the compliance with strength and deformation, crashworthiness and flutter behavior requirements. General view of the sailplane LAK-17B is shown in Fig. 1.

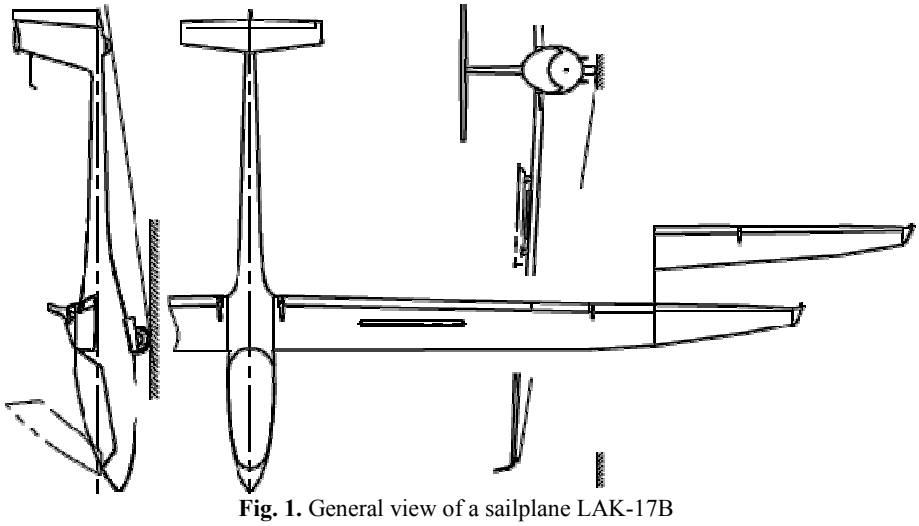

Fig. 1. General view of a sailplane LAK-17B

LAK-17B is a modification of a certified sailplane LAK-17A. Compliance with strength requirements of this sailplane was confirmed by load tests. Data of these tests will be used to evaluate reliability of the numerical model. The paper provides modeling principles that were used to construct FE models of the sailplanes LAK-17A and LAK-17B. Load evaluation procedure is also described.

To be able to compare results of two numerical calculations, the same load evaluation procedure was used for both finite element models. The loads were calculated for minimal and maximal sailplane weight, for all flaps positions and all flight conditions of the *V-n* diagram. A chart of velocity versus load factor, or *V-n* diagram indicates the limits of aircraft performance. It shows how much load factor can be safely achieved at different airspeeds. The maneuvering speed V_A of an aircraft is an airspeed limitation selected by the designer or the aircraft. At speeds close to, and faster than the maneuvering speed, full deflection of any flight control surface should not be attempted because of the risk of damage to the aircraft structure.

Experimental data was used to verify modeling results. Two types of static test results were supplied by the manufacturer of the sailplane: displacements of the horizontal stabilizer specific points and strains at specific points of the fuselage shell structure.

Finite element model

Finite element model of the fuselage was constructed using MSC.Patran software [5]. The CAD-model used for meshing was created in external CAD software and surface data was imported to MSC.Patran environment. CAD modeling process was performed in two stages. At first, a wireframe structure of the fuselage and tail surfaces was created using spline curves. At the second stage, the wireframe was covered with bi-parametric surfaces.

Standard meshing tools of MSC.Patran software was used. Four-node two-dimensional elements (QUAD4) were used to model composite parts of the sailplane. Three-node elements (TRIA3) were only used to model the trailing edges of aerodynamic surfaces and to ensure mesh transition. The general view of stabilizer and fuselage FE models is illustrated in Fig. 2 and Fig. 3.

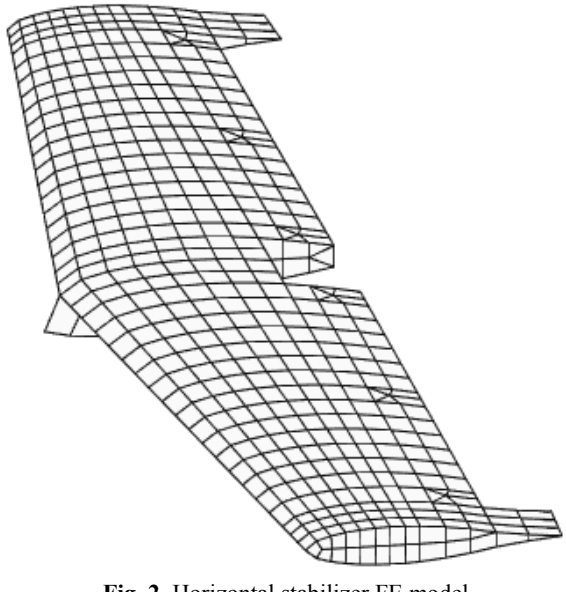

Fig. 2. Horizontal stabilizer FE model

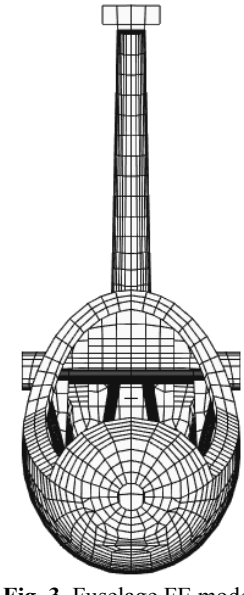

Fig. 3. Fuselage FE model

Load evaluation

In order to compare results of two numerical calculations, the same load evaluation procedure must be applied for both FE models. Calculation of fuselage loads was performed in two planes: vertical and horizontal when stabilizer and fin loads are acting together.

Fuselage calculation scheme (Fig. 4) consists of two-support beam, which is loaded by the fuselage weight, pilot weight, stabilizer load and aero towing load. The beam supports are pins connecting wing and fuselage.

If stabilizer or towing hook loads increases suddenly, they are compensated by inertia forces (Fig. 4).

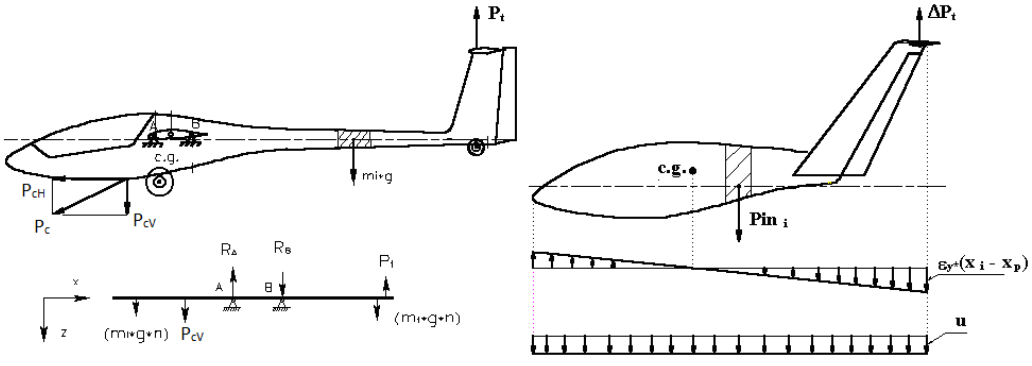

Fig. 4. Scheme of evaluation of fuselage loads: P_c - towing cable load; m_i - distributed fuselage mass; P_t - stabilizer balancing load; ε_y - sailplane angular acceleration; ΔP_t - change of stabilizer aerodynamic load; x_i - coordinate of distributed mass center; x_p - distance between sailplane nose and stabilizer mass center; u - sailplane linear acceleration; P_{in} - distributed mass inertia force

For sailplanes where the horizontal tail is supported by the vertical tail, the tail surfaces and their supporting structure including the rear portion of the fuselage should be designed to withstand the prescribed loadings on the vertical tail and the rolling moment induced by the horizontal tail acting in the same direction. Reference [1] suggests that for T-tails in the absence of a more rational analysis, the rolling moment induced by the side-slip or deflection of the vertical rudder may be computed as follows:

$$M_r = 0.4 S_t \frac{\rho_0}{2} \beta V^2 b_V \tag{1}$$

where M_r is induced rolling moment at horizontal tail, b_V is span of vertical tail, measured from the bottom of the fuselage, β is side-slip angle.

The (1) formula is only valid for vertical tail aspect ratios between 1 and 1.8 and horizontal tail with no dihedral and aspect ratio 6 or less.

Air gust loads on vertical tail surfaces were calculated using the following equation [1]:

$$P_f = a_v S_f \frac{\rho_0}{2} VUk \tag{2}$$

where P_f is gust load, a_v is slope of vertical tail lift curve per radian, S_f is area of vertical tail, ρ_0 is density of air at sea level, V is speed of flight, U is gust speed, k is gust factor.

The rolling moment induced by gust load was calculated as follows:

$$M_r = 0.4 S_t \frac{\rho_0}{2} V U b_V k \tag{3}$$

The unsymmetrical distribution of the balancing load on the horizontal tail which arises in flight conditions *A* and *D* of the *V-n* envelope was combined with the appropriate maneuvering load on the vertical surface as specified in [1] acting in such a direction as to increase the rolling torque. In the absence of rational data the unsymmetrical distribution was obtained by multiplying the air load on one side of the plane of symmetry by $(1+x)$ and on the other side - by $(1-x)$. For point *A* of the *V-n* envelope the value of *x* shall be 0.34 and for point *D* the value of *x* shall be 0.15 [1]. During calculation of the unsymmetrical distribution of the balancing load on the stabilizer, the unsymmetrical horizontal tail load was not combined with the induced rolling moment at the T-tail. The loads were calculated for minimal and maximal sailplane weight, for all flaps positions and all flight conditions of the *V-n* envelope. The calculation results are depicted graphically in Fig. 5.

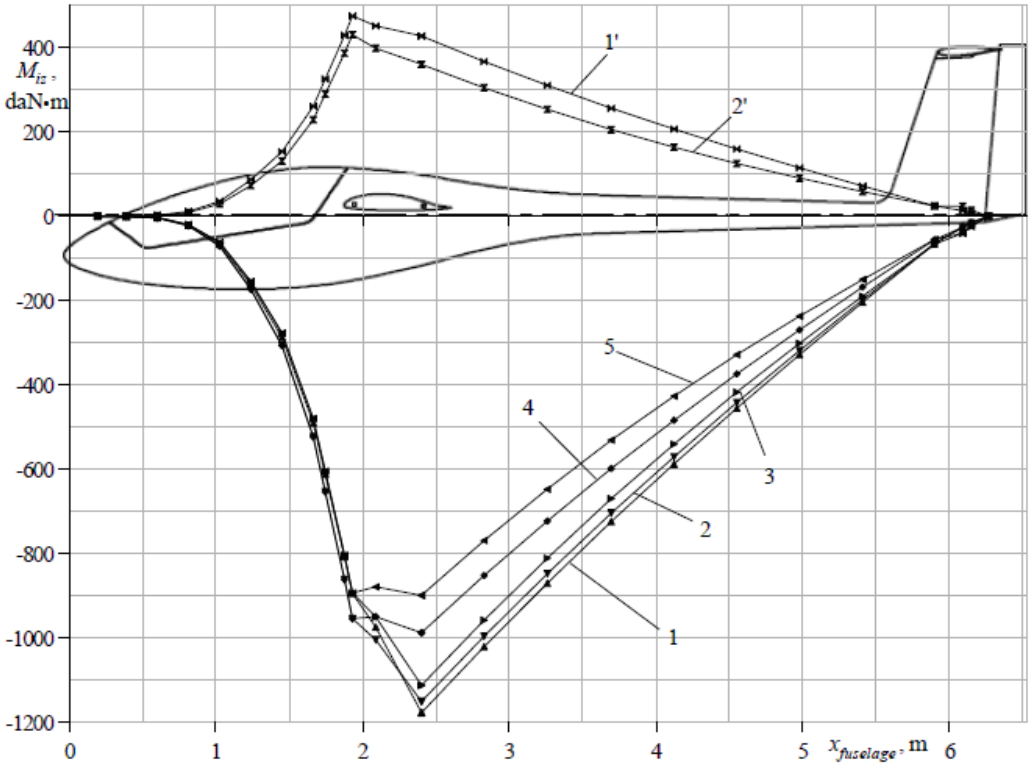

Fig. 5. Diagram of maximal and minimal bending moments of sailplane LAK-17A fuselage: 1 - case *D*, *m* = 330 kg, *V* = 224 km/h, flaps 10^0, load factor *n* = 6.85; 2 - case *A*, *m* = 330 kg, *V* = 190 km/h, flaps 10^0, load factor *n* = 7.31; 3 - case *A*(1-n_1), *m* = 330 kg, *V* = 206 km/h, flaps 10^0, load factor *n* = 7.31; 4 - case *A*, *m* = 330 kg, *V* = 206 km/h, flaps -5^0, load factor *n* = 7.31; 5 - case *A*(1-n_1), *m* = 330 kg, *V* = 206 km/h, flaps -5^0, load factor *n* = 7.31; *1'* - case *G*, *m* = 330 kg, *V* = 178 km/h, flaps -5^0, load factor *n* = -3.64; *2'* - case *A*(1-n_4), *m* = 330 kg, *V* = 206 km/h, flaps -5^0, load factor *n* = -3.64

Fig. 5 reveals that that curves 1) and 2) represent the most critical loading conditions of the fuselage rear and front parts.

The theoretical loads acting on fuselages of sailplanes LAK-17A and LAK-17B as well as tail surfaces are provided in Table 1. These loads were applied to the fuselage finite element model according to distribution scheme in Fig. 6.

Table 1. Theoretical loads acting on sailplanes LAK-17A and LAK-17B

	Sailplane LAK-17A				Sailplane LAK-17B			
	Loading in vertical plane		Combined loading on tail surfaces		Loading in vertical plane		Combined loading on tail surfaces	
Index	Case *A*	Case *D*	$U = 15$ m/s, $V = V_A$	1/3 of max rudder deflection, $V = V_D$	Case *A*	Case *D*	$U = 15$ m/s, $V = V_A$	1/3 of max rudder deflection, $V = V_D$
*P*1, daN	4.19	3.94	4.19	3.94	3.78	3.38	3.78	3.38
*P*2, daN	10.56	9.9	10.56	9.9	11.34	10.13	11.34	10.13
*P*3, daN	73.56	68.95	73.56	68.95	64.26	57.39	64.26	57.39
*P*4, daN	138.18	129.52	138.18	129.52	122.86	109.71	122.86	109.71
*P*5, daN	256.79	240.7	256.79	240.7	222.07	198.32	222.07	198.32
*P*6, daN	143.64	134.64	143.64	134.64	142.7	127.43	142.7	127.43
*P*7, daN	387.93	363.61	387.93	363.61	335.49	299.6	335.49	299.6
*P*8, daN	573.46	537.52	573.46	537.52	533.95	476.82	533.95	476.82
*P*9, daN	129.04	120.95	129.04	120.95	113.41	101.27	113.41	101.27
*P*10, daN	151.79	142.27	151.79	142.27	167.27	149.38	167.27	149.38
*P*11, daN	91.99	86.23	91.99	86.23	146.48	130.81	146.48	130.81
*P*12, daN	18.67	17.5	18.67	17.5	462.13	412.68	462.13	412.68
*P*13, daN	13.32	12.48	13.32	12.48	11.34	10.13	11.34	10.13
*P*14, daN	19.6	18.37	19.6	18.37	17.01	15.19	17.01	15.19
*P*15, daN	9.89	9.27	9.89	9.27	9.45	8.44	9.45	8.44
*P*16, daN	13.31	12.47	13.31	12.47	11.34	10.13	11.34	10.13
*P*17, daN	7.64	7.16	7.64	7.16	6.62	5.91	6.62	5.91
*P*18, daN	6.6	6.19	6.6	6.19	5.67	5.06	5.67	5.06
*P*19, daN	76.82	72.01	76.82	72.01	66.15	59.08	66.15	59.08
*P*20, daN	44.61	41.82	44.61	41.82	118.13	105.49	118.13	105.49
*P*21, daN	135.53	127.04	135.53	127.04	38.75	34.6	38.75	34.6
Pt, daN	27.54	-42.28	27.54	-42.28	-13.83	-113.05	-13.83	-113.05
Pv, daN	0	0	245.34	201.11	0	0	283.1	250.48
Mr, daNm	0	0	27.44	22.49	0	0	27.14	24.02

Data of static tests

Experimental data was used to verify modeling results. Two types of static test results were supplied by the manufacturer of the sailplane: displacements of the horizontal stabilizer specific points and strains at specific points of the fuselage shell structure.

During the test, the stabilizer and fuselage were loaded by steps up to the limit loads (the maximum loads to be expected in service), increasing the load by 10 % in each step.

Displacements of the stabilizer structure in vertical plane were measured using mechanical devices. The measurement scheme is illustrated in Fig. 7.

Measurement results for horizontal stabilizer displacements are listed in Table 2. Displacements of two points located at 960 mm distance from symmetry plane of the stabilizer were obtained.

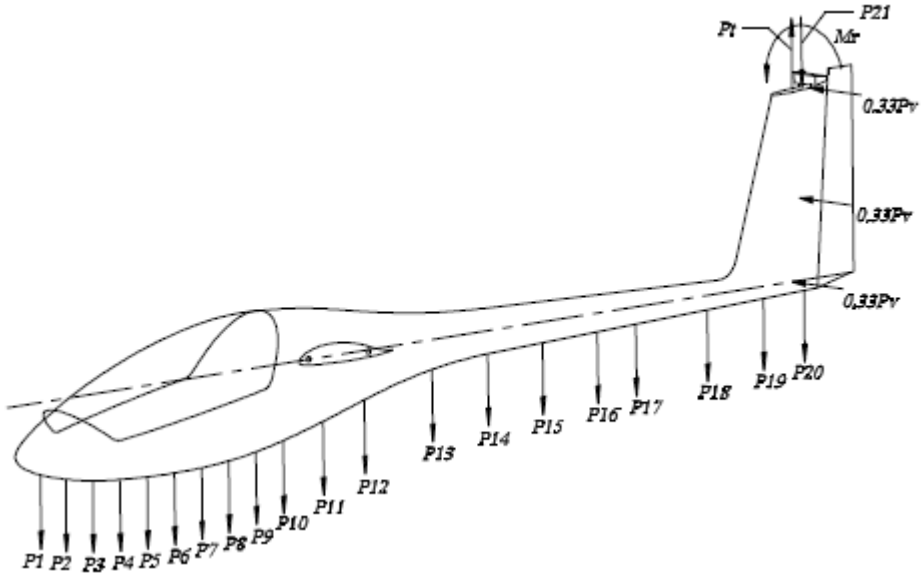

Fig. 6. Scheme of load distribution in the finite element model

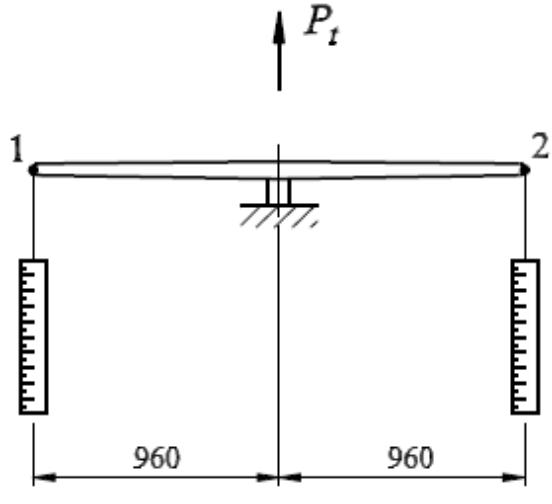

Fig. 7. Scheme of measurement of stabilizer displacements

Table 2. Horizontal stabilizer test results

No.	Load P_t, %	Displacement u, mm	
		1st ruler	2nd ruler
1	0	0	0
2	10	3	3
3	20	7	8
4	30	10	12
5	40	14	16
6	50	17	20
7	60	21	23
8	67	24	27

The strains were measured in five parallel sections of the fuselage. Electrical measurement devices were used to evaluate the strains at specific points on the fuselage shell. The scheme of arrangement of all the strain gauges is depicted in Fig. 8.

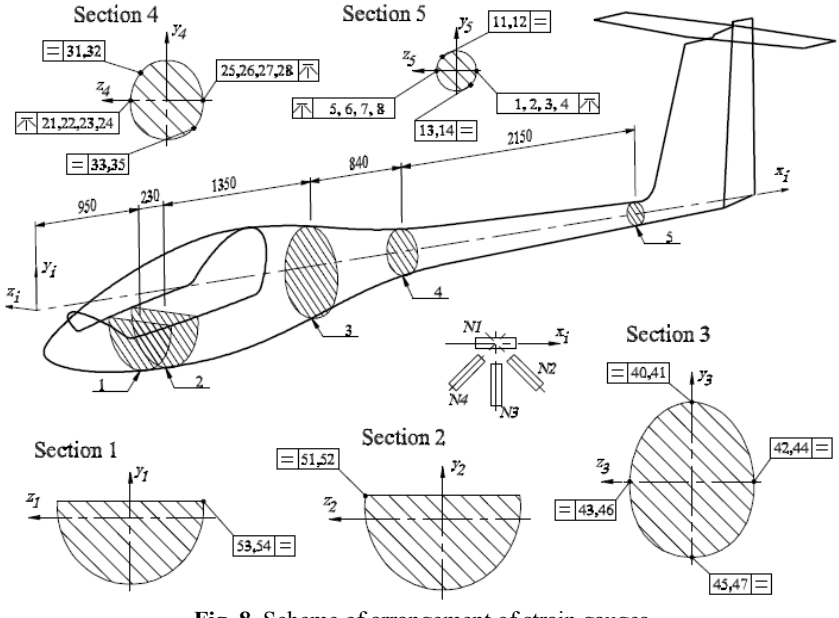

Fig. 8. Scheme of arrangement of strain gauges

Numerical results

MSC.Nastran [6] software was used to simulate the critical regimes of sailplanes LAK-17A and LAK-17B structures. Analysis of results was performed using MSC.Patran post-processing tools.

To simulate different flight conditions, analytically calculated loads (Table 1) were applied to the fuselage and horizontal tail finite element models. Loads distribution scheme is illustrated in Fig. 6.

Experimental data of the stabilizer static tests was used to verify modeling results (Fig. 9).

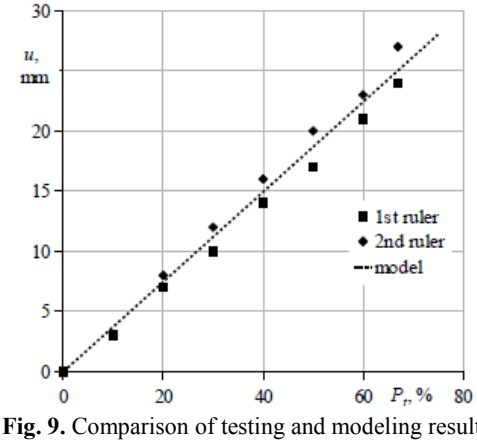

Fig. 9. Comparison of testing and modeling results

Displacements values of two nodes located at 960 mm distance from symmetry plane of the stabilizer model were obtained. At present stage of model development process, the modeling results are considered acceptable.

The strains were measured in fourth and fifth sections of the fuselage (see Fig. 8). Strain values at four positions of the finite element model were obtained and are compared in Table 3.

Table 3. Numerically obtained strains

	Strain ε, %	
Strain gauge No.	LAK-17A	LAK-17B
1	0.168	0.205
2	-0.062	-0.077
3	-0.111	-0.134
4	0.119	0.148
5	-0.152	-0.187
6	-0.178	-0.213
7	0.093	0.115
8	0.119	0.141
21	-0.087	-0.114
22	-0.067	-0.083
23	0.022	0.014
24	0.001	-0.017
25	0.212	0.26
26	0.046	0.041
27	-0.034	-0.058
28	0.133	0.162

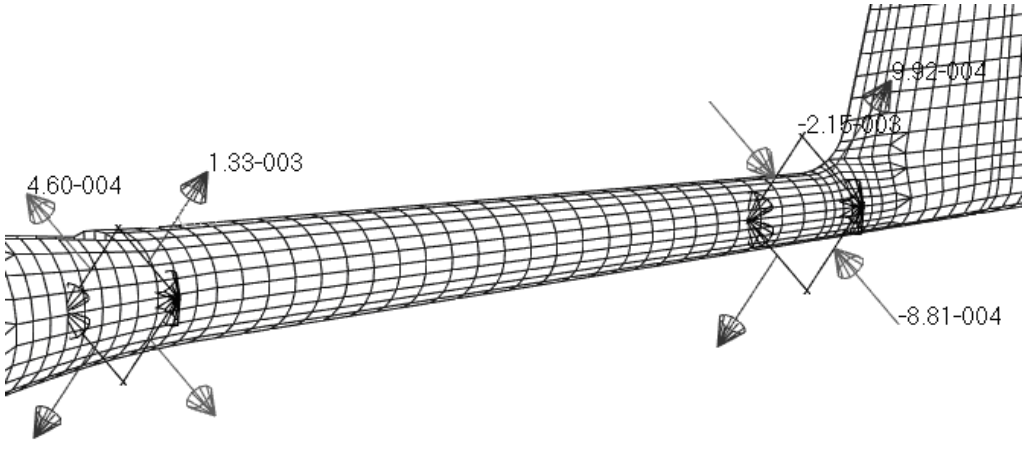

Fig. 10. Preview of strain calculation results

In future work the obtained results will be compared to values measured by strain gauges.

Conclusions

Loads calculation results indicate that the most critical load cases for sailplane LAK-17A occurs at points *A* and *D* of the *V-n* envelope, when the sailplane mass is 330 kg and the flaps are in position "$+10^0$" at speeds 224 km/h (case A) and 190 km/h (case D).

At present stage of model development process, the modeling results of the sailplane horizontal tail are considered acceptable, however, results convergence tests must be performed in the future.

References

[1] EASA. Certification Specifications for Sailplanes and Powered Sailplanes CS-22, 2009.
[2] **Hollmann M.** Modern Aerodynamic Flutter Analysis. Monterey, CA, Aircraft Designs, Inc., 1991, 160 p.
[3] **Vijaya Vittala N. G., Swarnalatha R., Pankaj A. C.** Dynamic and aeroelastic analysis of a transport aircraft. Int. Conf. on Aerospace Technologies, Indian Institute of Science, Bangalore, 2008, p. 26-28.
[4] **Wright J. R., Cooper J. E.** Introduction to Aircraft Aeroelasticity and Loads. Willey, John & Sons, Ltd., 2007, 526 p.
[5] MSC.Patran Users Manual. MSC.Software Corporation, CA, 1999.
[6] MSC.Nastran User's Manual. Version 66, The MacNeal-Schwendler Corporation, Los Angeles, CA, November 1988.
[7] **Zienkiewicz O. C., Taylor R. L.** Finite Element Method - The Basis. Oxford: Butterworth-Heinemann, 2000, 689 p.
[8] **Stockwell A. E.** Simulation of an Impact Test of the All-Composite Lear Fan Aircraft. NASA CR 2002-211458, June 2002.
[9] **Jackson K. E., Fasanella E. L., Boitnott R. L., Lyle K. H.** Full-Scale Crash Test and Finite Element Simulation of a Composite Prototype Helicopter. NASA/TP-2003-212641, ARL-TR-2824, August 2003.
[10] **Vijaya Vittala N. G., Pankaj A. C., Venkatasubramanayam D. V.** Flutter analysis of a composite light trainer aircraft. Journal of Scientific & Industrial Research, Vol. 69, February 2010, p. 113-120.